33RD CONGRESS
OF THE INTERNATIONAL COUNCIL
OF THE AERONAUTICAL SCIENCES
STOCKHOLM, SWEDEN, 4-9 SEPTEMBER, 2022

ICAS 2022 SWEDEN

WALL INTERFERENCE CORRECTIONS USING NONLINEAR LEAST-SQUARES OPTIMISATION

Simon Noel[1], David M. Birch[2], John J. Doherty[2] & Tanmay Tipnis[1]

[1]QinetiQ Ltd., Farnborough, United Kingdom, GU14 0LX
[2]University of Surrey, United Kingdom

Abstract

A novel approach to correcting the effects of wall interference has been developed for closed-wall wind tunnels using a nonlinear least squares optimisation process that is independent of model geometry. Potential flow singularities are used to represent the test object and the method of images is used to represent the tunnel walls. The present approach makes use of trust-region reflective optimisation to allow the locations and strengths of singularities to be determined iteratively with only wall pressure measurements as independent inputs. The technique has been validated using CFD simulations of flow around canonical shapes in both free and wall-bounded conditions at blockages of 5 % to 20 %. Comparisons are drawn to the two-variable method, with demonstrated improvements across the range of bodies considered.

Keywords: wind tunnel, wall interference, optimisation

1. Background

A major source of error in wind tunnel testing arises from the interference effects between the wind tunnel walls and the test model. In a closed-wall tunnel, boundary layer growth along the walls results in a pressure gradient along the length of the tunnel referred to as horizontal buoyancy [1] - although the effects of this are typically mitigated through facility design. For a lifting model, the general redirection of the flow downwards is constrained by the tunnel floor, resulting in an induced upwash known as lift interference. The walls also impose a flow constraint in the region around the model and its wake, causing a local increase in streamwise velocity, affecting the aerodynamic forces and moments experienced by the model. It is imperative that wind tunnel test data be corrected for these effects, as aircraft design demands very low uncertainty from wind tunnel data [2].

One of the most widely-used correction techniques in wind tunnel testing is the two-variable (2V) method [3]. By defining a control volume bounded by the tunnel walls and by arbitrary upstream and downstream planes, the strength of all sources and sinks representing the tunnel walls can be obtained from the potential flux using the divergence theorem. To obtain a unique solution, two independent flow variables at the bounding surface are needed: for closed wall tunnels this may be taken as the streamwise velocity, and wall-normal velocity equal to zero due to the assumed impermeability of the walls. The key advantage of this technique is that it can determine the interference flow field independently of any model representation. However, in order to do this, this technique normally requires a large number of wall pressure measurements (typically $n \approx 100$) in order to obtain a sufficiently resolved solution.

Contrary to the approach taken by the 2V method, the wall pressure signature technique provides estimates of the interference flow field by modelling the object in the wind tunnel and its wake as the superposition of source, sink and doublet elements centrally located along the tunnel axis [4]. This technique has the advantage of requiring significantly fewer measurements to obtain a unique solution (typically, $n \lesssim 20$ [5]). However, the wall pressure-signature technique does not capture upwash corrections particularly well, as the blockage is assumed to be axisymmetric. The technique

can be improved by moving the singularities off of the centreline, but this requires that the particular locations of the singularities be known *a priori* [6].
The technique has been extended to accommodate off-centre singularities, horseshoe vortices, and model forces [7]. Other implementations have included the use of statistical techniques to obtain the singularity characteristics from an over-prescribed boundary condition, thereby allowing the use of additional wall pressure measurements to improve the fit [8], and the use of panel-method representations of the tunnel walls to facilitate corrections within wind tunnels of arbitrary cross-sectional geometry [9].
Despite these advancements, the wall pressure-signature method still requires the type, location and strength of the singularity to be prescribed, relying on either empirical observations or engineering experience.
The developments in the present work build upon that of panel code ANTARES used in the NASA Ames Transonic facility [8], [10] whereby a 'global' least squares fit matches the wall pressures across all wall ports using potential singularities. The Wall Interference Correction System (WICS) method represents the model as a series of point sources, sinks and line doublets as with the wall signature method and determines the singularity strengths from the wall velocities [9]. Furthermore, it can more readily evaluate the effects of strut interference by evaluating the strut independently of the model and superimposing the interference field on that of the model. However, this approach still requires the wind tunnel engineer to prescribe the initial positions of the singularities, with limited freedom for the singularities to move. For example, where a fuselage is represented by a point source and sink (a rankine body), this method allows the singularities to move along a linear path between the two locations.

2. Problem formulation

Because the models being tested are typically located far enough from the wind tunnel walls to minimise boundary layer interaction, wall correction methods generally assume that the wall interference causes small perturbations to the flow and will not result in any viscous interactions with the model. This concept has been used to approach wind tunnel wall interference using potential theory for the better part of a century [11]. The specific influence of the walls on the flow around the model may therefore be approximated by assuming the flow to be irrotational, incompressible and inviscid [5], making use of the Prandtl-Glauert transformation $\beta = \sqrt{1-M_\infty^2}$ where M_∞ is the freestream Mach number, to linearise the effects of compressibility. Note that the free-stream Mach number M_∞ is defined as the far-field upstream Mach number in the absence of constraining walls. Under these assumptions, the effects of the test model on the flow can be reproduced through the superposition of some number of potential flow singularities, and the effects of the walls on the flow can be approximated using the method of images. The locations and strengths of the singularities (and their images) then uniquely define the velocity potential function $\phi(x,y,z)$, such that

$$\beta^2\frac{\partial^2\phi}{\partial x^2}+\frac{\partial^2\phi}{\partial y^2}+\frac{\partial^2\phi}{\partial z^2}=0 \tag{1}$$

where the velocity components may be obtained from the continuity equation as $u=\partial\phi/\partial x$, $v=\partial\phi/\partial y$ and $w=\partial\phi/\partial z$. The proceeding content of this paper considers two-dimensional cases, and will refer to the streamwise and vertical directions as x,y, respectively, with corresponding velocity components u,v.
To illustrate this method, consider a two-dimensional domain in (x,y), transformed into polar coordinates about $(0,0)$. At an arbitrary (r,θ) take a point doublet with some radius R and circulation Γ. Then the velocity potential ϕ for a doublet situated in a uniform flow with a velocity of U_∞ is given as [12]

$$\phi=U_\infty\sin\theta r\left(1-\frac{R^2}{r^2}\right)+\frac{\Gamma}{2\pi}\ln\frac{r}{R} \tag{2}$$

Taking the velocity in polar coordinates as

$$u_r=\frac{1}{r}\frac{\partial\phi}{\partial\theta}\qquad u_\theta=-\frac{\partial\phi}{\partial r} \tag{3}$$

where ∂ refers to the partial derivative, the potential equations can be expressed as

$$u_r = U_\infty \cos\theta \left(1 - \frac{R^2}{r^2}\right) \tag{4}$$

$$u_\theta = -U_\infty \sin\theta \left(1 + \frac{R^2}{r^2}\right) - \frac{\Gamma}{2\pi r} \tag{5}$$

By applying the transformation into Cartesian coordinates as

$$\begin{pmatrix} u \\ v \end{pmatrix} = \begin{pmatrix} \cos\theta & -\sin\theta \\ \sin\theta & \cos\theta \end{pmatrix} \begin{pmatrix} u_r \\ u_\theta \end{pmatrix} \tag{6}$$

and by representing the radius of the cylinder R by the strength of the doublet as

$$R^2 = \frac{\kappa}{2\pi U_\infty} \tag{7}$$

equations 4 and 5 can be expressed as

$$u = \left(U_\infty - \frac{\kappa}{2\pi r^2}\cos 2\theta\right) - \frac{\Gamma \sin\theta}{2\pi r} \tag{8}$$

$$v = -\frac{\kappa}{2\pi r^2}\sin 2\theta + \frac{\Gamma\cos\theta}{2\pi r} \tag{9}$$

In order to solve for κ and Γ, equations 8 and 9 can now be expressed as

$$\begin{pmatrix} U_\infty - \frac{1}{2\pi r^2}\cos 2\theta & -\frac{\sin\theta}{2\pi r} \\ -\frac{1}{2\pi r^2}\sin 2\theta & \frac{\cos\theta}{2\pi r} \end{pmatrix} \begin{pmatrix} \kappa \\ \Gamma \end{pmatrix} = \begin{pmatrix} u \\ v \end{pmatrix} \tag{10}$$

This equation is now of the form $\mathbf{Ax} = \mathbf{b}$ and the singularity strengths can be determined by using standard linear algebra. It should be noted that in the case of wind tunnel experiments, any number of measurement locations may be used, meaning $\mathbf{A}$ may not necessarily be square and therefore invertible. As such, this system of equations is typically solved using singular value decomposition [8].

Having solved equation 10, the correction procedure can be applied. The difference between the velocity fields with and without the effect of the walls is typically described in the form of the blockage factors δ and ε, such that

$$\begin{aligned} \delta &= \frac{\Delta v}{U_\infty} \\ \varepsilon &= \frac{\Delta u}{U_\infty} \end{aligned} \tag{11}$$

where U_∞ is the freestream velocity magnitude. Classically, ε is taken to be the sum of the from the solid blockage ε_s and the wake blockage ε_w.

Under the inviscid far-field assumptions of small perturbations (and assuming again that u dominates over v and w), the streamwise wall velocity perturbations can be obtained from the linearised Bernoulli equation as

$$\frac{\Delta u}{U_\infty} = -\frac{1}{2}\Delta C_p \tag{12}$$

where C_p denotes the usual pressure coefficient. Taking the interference velocities in eq. 11 along the model centreline, the drag and lift coefficients (C_D, C_L) may then be corrected as

$$C_{Dc} = \frac{C_{Du} - \delta C_{Lu}}{(q_c/q_u)} \tag{13}$$

$$C_{Lc} = \frac{C_{Lu} + \delta C_{Du}}{(q_c/q_u)} \tag{14}$$

where the subscripts *c* and *u* refer to the corrected and uncorrected quantities, respectively and q is the dynamic pressure.

2.1 Nonlinear least-squares correction method

Given the current low cost of computing power, it should be possible to implement a modified wall-pressure signature technique whereby only the number and type of singularities are fixed, while the locations and strengths are obtained by fitting to the available wall-pressure data. This should enable the corrections to better represent complex or even unknown geometries, and yield more accurate, consistent corrections.

This work builds upon that of Ulbrich et. al [13] by removing the constraint for fixed singularity position and type. As opposed to relying on the test engineer to select appropriate singularities to represent the test article with limited scope for movement of singularities, this method uses nonlinear optimisation to achieve a representation of the interference flow field. Referring back to equation 10, the positions (r,θ) (or (x,y) in the usual Cartesian format) are also considered variables, and it is clear that the equations cannot be linearised in $[x,y,\kappa,\Gamma]$ and solved analytically.

The approach taken in this work makes use of the trust-region-reflective nonlinear least-squares algorithm [14], [15] implemented using the inbuilt *MATLAB lsqnonlin* functionality. This optimisation technique has been developed for the purpose of locating a local minimiser of a smooth nonlinear function with bounded variables. This algorithm is a Newton optimisation technique, meaning it makes use of the second partial derivatives (Hessian matrix) of the inputs to arrive at a solution, and by using the curvature of the space to arrive at the solution, it yields faster convergence. This requires that the objective function is twice continuously differentiable which is satisfied for potential singularities.

The trust-region reflective algorithm defines a "trust region" χ whereby the objective function to be minimised can be approximated as a quadratic function. A perturbation is then applied to the parameter in question. If the resulting change in the objective function exceeds the trust-region, χ is reduced and the process repeated. This ensures that sufficiently small steps are taken during the process to achieve a global and local quadratic convergence [15]. Here, the objective function is comprised of the sum of squares of the set of measured wall velocities in equation 12 subtracted from the velocities derived from the method of images.

The set of upper and lower bounds in this application are given in Table 1 below. L,H refer to the tunnel length and height respectively. The constraints of primary importance for this application are the requirements for the positions of the singularities to be located in the confines of the tunnel. The upper bound of κ is determined from the equation for doublet radius given in equation 7. The initial values given in brackets are randomly distributed between 0 and the upper bound given with the exception of x_0 where the starting values are hyperbolically spaced between $-L/2$ and $L/2$.

Table 1 – Least-squares constraints and initial values

Variable	Lower Bound	Upper Bound	Initial Value
x	$-L/2$	$L/2$	$[-L/2, L/2]$
y	$-0.49H$	$0.49H$	0
κ	0	$2\pi V_\infty (H/3)^2$	$[0, 2\pi V_\infty (H/10)^2]$
Γ	$-\infty$	∞	$[0, 10^{-4}]$

The Nonlinear Least Squares (NLSQ) algorithm is applied following the process shown in Figure 1. There are two inputs to the algorithm: the measured wall velocities (at present evaluated using CFD), and an initial guess of the positions, doublet strength, and circulation $[x_0, y_0, \kappa_0, \Gamma_0]$ for each point doublet used to represent the test article. At present, sources and sinks are not considered. The method of images is applied to the potential flow equations for the initial distribution of singularities. The Prandtl-Glauert transformation is applied [16] and the velocities are calculated at the same locations as the measured velocities. The objective function - the sum of squared differences between the measured and calculated velocities, is then passed to the *lsqnonlin* algorithm where the initial values are perturbed subject to the upper and lower bounds of each variable defined in Table 1. The trust-region reflective algorithm is then iteratively used to determine the strengths and positions of the singularities which minimise the objective function, providing the best match between the method of images and measured wall velocities. Finally, the optimal singularities are used to solve the potential flow equations at the desired test locations as input to eq. 11. The algorithm is able to calculate the interference correction in the order of one minute on a standard desktop machine.

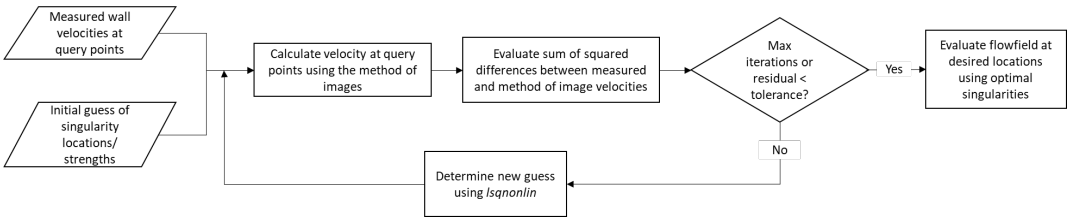

Figure 1 – Flow diagram of the NLSQ iterative procedure

An example arrangement of singularities is shown in Figure 2 for a 2D cylinder at Reynolds number $Re = 10^6$ and a height/diameter (H/D) equal to 5. The figure shows a free-air representation of the cylinder calculated using CFD, with flow from left to right. Doublets (dipoles) are freely distributed throughout the domain in order to achieve the same wall bounded velocity profile, and the walls are removed to determine the equivalent free-air profile. There is little disturbance upstream of the body, illustrated by the sparse distribution of small doublets. At the model location and its wake bubble, there is a cluster of doublets of larger strength (larger radius), forcing the wall bounded flow to achieve a higher velocity. Finally, the long tail of the wake results in a wall velocity greater than the free-stream, represented by the broadly equal strength doublets periodically located downstream.

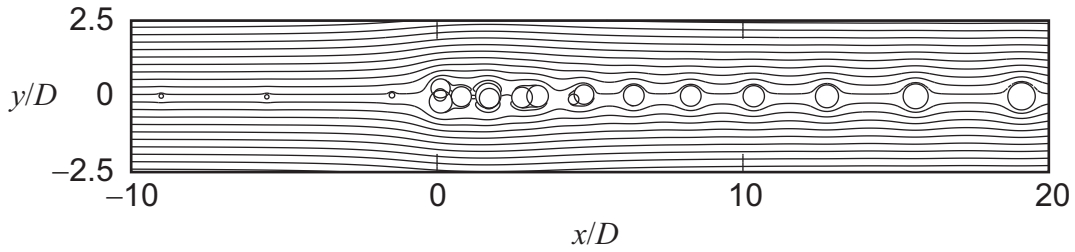

Figure 2 – Streamlines for NLSQ representation of a static 2D cylinder at $Re = 10^6$, $H/D = 5$

2.2 Assessment using CFD simulations

The challenge in developing a wall interference correction method arises when determining the benchmark against which the corrections are to be assessed. Whereas wind tunnel experiments capture the physics, it is rarely possible to also experimentally obtain a free-air equivalent to the wall bounded flow. Hence, the effectiveness of the nonlinear least-squares correction method has been demonstrated using data from CFD simulations of canonical 2D geometries in the presence and absence of walls. Data were collected for $H/D = 5, 10$ and 20. The geometries tested included a cylinder, a NACA 0012 aerofoil with and without a spoiler, and a NACA 4415. It should be noted that the H/D for the aerofoils is defined using the body chord.

CFD simulations were carried out using the ANSYS Fluent solver. 2D simulations were evaluated on a domain measuring $800D$ in length and $400D$ in height, as shown in Figure 3. The large domain is used to represent the free-air condition, with subset regions of the domain used for each wall bounded condition, as indicated by the horizontal lines labelled as $H/D = 2, 5, 10, 20, 50$. The flow enters the domain through a mass flow inlet on the left hand side of the figure and exits via the pressure outlet at atmospheric pressure. The farfield walls in the unbounded domain are represented by velocity boundaries at the same velocity as the mass flow inlet. The curved boundaries have been chosen to allow the flow to either enter or leave the domain at an angle that is not tangent to the boundary. At each H/D, the domains outside the required H/D are deleted, and the outermost wall is defined as a slip-wall, i.e. zero shear-stress. At this stage it is unnecessary to include no-slip walls as it can be assumed that a buoyancy correction has already been applied to the data, independently of the wall correction procedure.

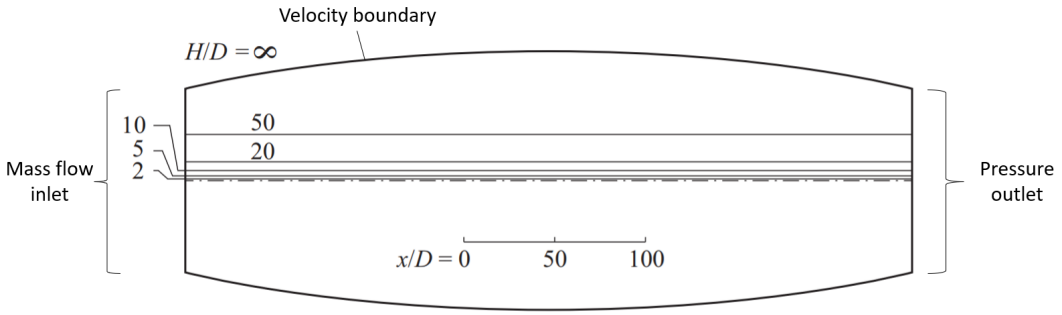

Figure 3 – Domain showing regions for $H/D = 2, 5, 10, 20, 50$ and Unbound cases

The steady-state Reynolds-Averaged Navier-Stokes (RANS) equations were solved using a second-order upwind Gaussian cell-based approach with a coupled pressure-velocity scheme. The flow is fully turbulent and laminar-turbulent transition has not been fixed in any case. The parameters used for each CFD simulation are shown in Table 2. The conditions have been pressure controlled to achieve the appropriate Reynolds number for a given Mach number.

Table 2 – CFD conditions for each body considered

Parameter	Cylinder	NACA 0012/NACA 4415	NACA 0012 Spoiler
Turbulence model	k-ε realizable	k-ω SST	k-ω SST
Re	$10^5/10^6$	10^6	$3.5 \cdot 10^5$
Mach	0.214	0.152	0.075
U_∞ (m/s)	73.0	51.94	25.56

CFD results have been validated against literature, with the 2D cylinder achieving $C_D = 0.374$ in the present study in comparison to $C_D = 0.39$ in [17], and Zdravkovich reporting values in the range $C_D = [0.17, 0.4]$ [18]. Lift and drag coefficients are displayed for the NACA 0012 and NACA 4415 results in Table 3. Results show consistency with that found in literature, with some deviation from expected values at high incidence for the NACA 4415. It should be noted that although confidence is required of the CFD results, for the purposes of determining the validity of the wall correction techniques, the relative accuracy with respect to the free-air flow is of greater importance. The NACA 0012 with deployed spoiler has been compared against two datasets. Letting c refer to the aerofoil chord length, the NACA 0012 with deployed spoiler follows the geometry and conditions in [19] consisting of a $10\%c$ spoiler on the upper surface from $0.7c$ to $0.8c$ with a $0.1\%c$ cavity. That study considered the effect of spoiler gaps at spoiler deflection angles ranging from 60° to 90° providing both steady state and transient data. Present results are evaluated at zero angle of attack and show excellent agreement with plotted values in the published work, as shown in the table. Further comparison is made to another study using the same geometry [20]. That study considered unsteady aerodynamics of a spoiler deploying from 0 up to 90°. Lower deflection angles are not comparable to this study as steady state does not read across to the dynamic motion of the spoiler. However, steady state results at 90° show reasonable agreement as follows: Present: $C_D = 0.08$, $C_L = 0.95$, [20]: $C_D = 0.13$, $C_L = -0.90$. Example pressure contours are shown in Figure 4 for the NACA 0012 with deployed spoiler at 45°, and NACA 4415 at zero incidence.

Table 3 – Validation of NACA CFD against literature

		C_D		C_L	
	Angle	Present	Literature	Present	Literature
NACA 0012 Ref. [21, 22]	0	0.008	0.009	0	0
	5	0.009	0.009	0.56	0.50
	10	0.013	0.012	1.10	1.10
	15	0.026	0.023	1.49	1.5
NACA 4415 Ref. [21]	0	0.009	0.008	0.48	0.45
	5	0.012	0.008	1.01	0.90
	10	0.017	0.016	1.46	1.45
	15	0.032	0.024	1.76	1.65
NACA 0012 Splr Ref. [19]	60	0.065	0.060	−0.85	−0.80
	90	0.080	0.100	−0.95	−1.00

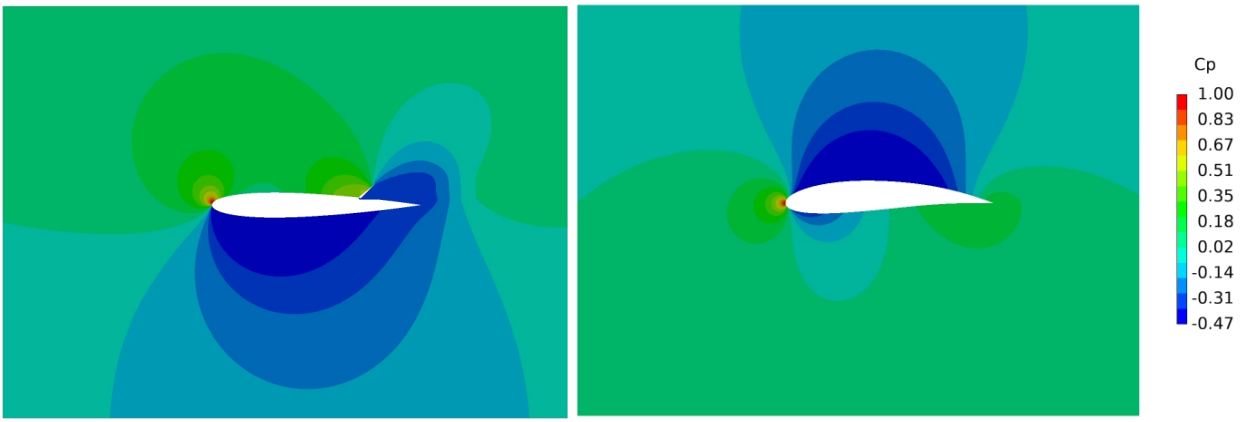

(a) NACA 0012 Spoiler 45° (b) NACA 4415

Figure 4 – Pressure contours over 2D aerofoils

3. Results

To test the effectiveness of the proposed NLSQ wall correction technique, optimal arrangements of inviscid singularities were generated to fit the bounded CFD data for each of the cases. The potential theory free-air domain is then calculated by removing the image walls and the results were used to correct the velocity fields, lift and drag obtained from the bounded velocity field. These corrected results could then be compared directly to the unbounded CFD.

3.1 2D cylinder

Figure 5 demonstrates the ability of the NLSQ algorithm to reproduce the far-field velocities around an arbitrary object and its viscous wake. Here, the locations and strengths of the singularities have been optimised to reproduce the flow around a 2D cylinder at $Re = 10^6$ and $H/D = 10$. The NLSQ algorithm has recovered the velocity profiles very well, particularly at the velocity peak. Furthermore, the $\Delta u/U_\infty$ required to give a $\Delta M > 0.001$ is approximately 0.004. The NLSQ velocity profile is within these bounds of the CFD profile everywhere, indicating that the method is performing well within typical wind tunnel tolerances.

The NLSQ technique has been directly compared to the 2V approach by evaluating the corrections returned by each method on upper and lower surfaces in 2D, each surface having 50 wall points. The 2V method is theoretically exact in the limit of an infinite number of points, and has been upsampled by a factor of 3 in the cases shown.

Figure 6 compares the resultant corrected velocities obtained using the present NLSQ technique and the classical 2V method. It is evident that there is little difference between the streamwise component of the free-air velocity using each approach, indicating near identical performance using

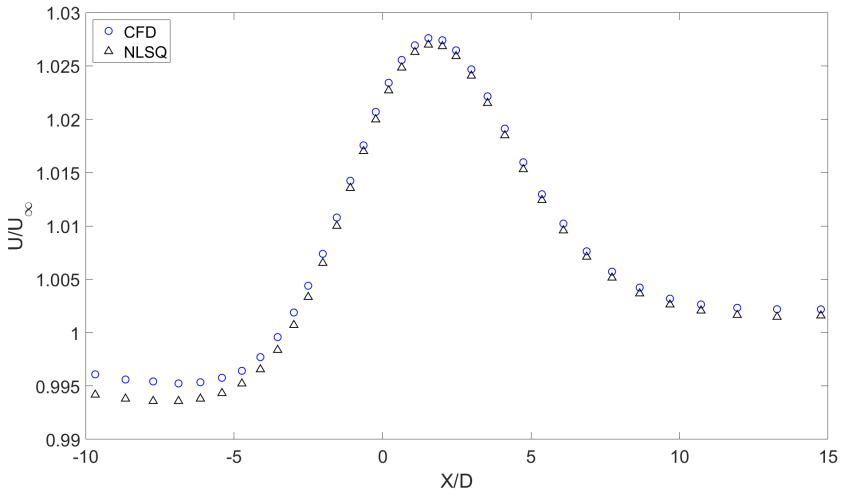

Figure 5 – Velocity magnitudes at top boundary CFD grid points for the case of a 2D cylinder with $Re = 10^6$, $H/D = 10$

each approach. Importantly, this comparison was made at 50% of the distance to the wall (rather than on the wall itself), as the 2V method is undefined at the walls.

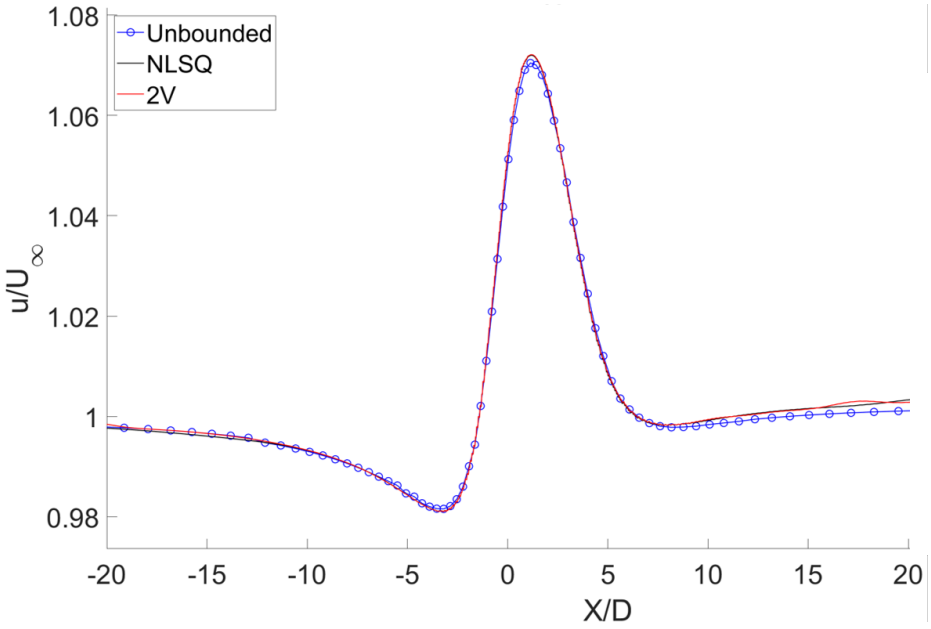

Figure 6 – Comparison of wall velocities around a 2D cylinder corrected using 2V and NLSQ methods at 75% tunnel height, with $Re = 10^6$ and $H/D = 10$

The differences between the corrected values of C_D and the equivalent unbounded values were compared are summarised in Table 4 for a range of Re and H/D. The measure of success is to achieve a value of zero, indicating that the technique has perfectly corrected to the free-air value. The Uncorrected column shows the difference between the bounded and free-air CFD as a benchmark. The current NLSQ correction moderately outperforms the 2V method in all cases aside from $H/D = 5$. It should be noted that this ratio represents a blockage of 20%, where typical practice considers models of $5 - 10\%$ blockage [23]. As the 2V method is implemented on a finite domain, it is able to better capture the blockage interference information as the magnitude of the interference increases [24]. However, the present method is superior as it can readily find an optimal arrangement of singularities to represent the wall bounded flow.

Table 4 – Difference between unbounded and bounded CFD results and between corrected and unbounded CFD results, 2D cylinder

		$\Delta C_D \times 10^4$		
Case	H/D	Uncorrected	NLSQ	2V
$Re = 10^5$	5	666	173	161
	10	165	30	32
	20	47	6.5	7.0
$Re = 10^6$	5	1497	447	438
	10	327	50	59
	20	95	3.0	13

3.2 2D Lifting bodies

In order to demonstrate the effectiveness of the NLSQ correction technique on the asymmetric flow fields (with significant up/downwash) of more relevance to generalised aerodynamic testing, flow around three aerofoils have been considered: a NACA 0012 aerofoil, a NACA 0012 aerofoil with deployed spoiler, and a NACA 4415 aerofoil with no spoiler. The NACA 0012 and NACA 4415 aerofoils have been evaluated at $\alpha = 0, 5, 10, 15$ degrees, with the NACA 0012 with spoiler evaluated at deployed angles of 45°, 60° and 90°. Throughout this section, H/D will be used to refer to the height/chord ratio as opposed to the diameter in previous sections.

Table 5 shows the difference in coefficient counts between the corrected data and the CFD free-air value for the NACA 0012 with deployed spoiler. As with the previous table, the objective is for the corrected values to obtain a value of zero. It should be noted that the drag coefficient is evaluated at a count of 10^4, whereas the lift coefficient is evaluated at a count of 10^3, as with typical wind tunnel test procedures. Furthermore, the table lists $-\Delta C_L$ as the spoiler generates negative lift. It is evident that across all spoiler configurations and blockage ratios, the present method has achieved a superior drag correction, where the 2V method has significantly over-corrected in some cases, resulting in an under-prediction of the true drag coefficient given by the negative values. The differences in C_L are marginal between the two methods, and are within one lift count, well within tolerances of repeatability of wind tunnel testing.

Table 5 – Difference between unbounded drag and lift counts from CFD and results from different corrections, for the case of a 2D NACA 0012 aerofoil with deployed spoiler

		$\Delta C_D \times 10^4$			$-\Delta C_L \times 10^3$		
Spoiler angle	H/D	Uncorrected	NLSQ	2V	Uncorrected	NLSQ	2V
45°	5	6.2	1.1	-1.1	15.7	8.0	7.5
	10	2.0	0.5	-5.8	4.9	2.4	1.8
60°	5	9.7	2.7	-2.7	21	9.0	8.6
	10	3.3	1.4	-8.3	6.7	2.8	2.1
90°	5	15	2.1	8.0	26	13	12
	10	5.1	0.6	9.4	8.6	3.9	3.1

Figure 7 shows the lift-drag polars at $H/D = 5$ for the NACA 0012 with no spoiler and Figure 8 shows the corresponding polars for the NACA 4415 at $H/D = 5$. The figures show the free-air (unbounded) CFD data in the dashed line along with the NLSQ and 2V corrected values in the solid lines. It is clear that the disparity between the free-air value and the respective corrected datasets increases with C_L (and therefore incidence). As the aerofoil incidence increases, the upwash and blockage interference increases, resulting in greater errors when applying each correction. However, it is clear that the corrected values of C_D using the NLSQ approach closely align with the free-air values whereas the 2V method has over-corrected the drag across all data points and cases.

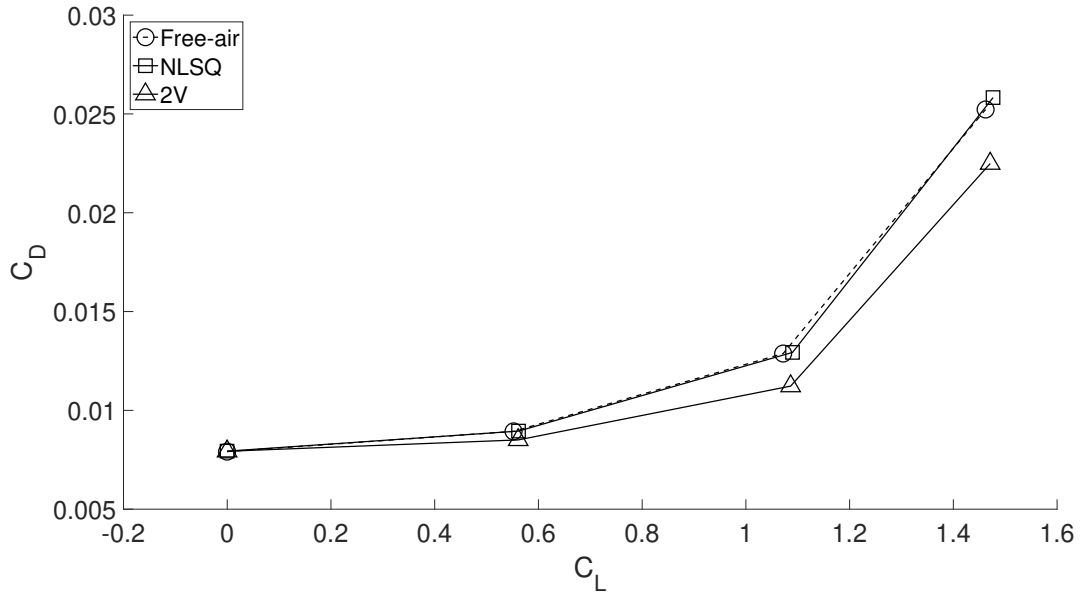

Figure 7 – Lift-Drag polars for the NACA 0012 at $H/D = 5$

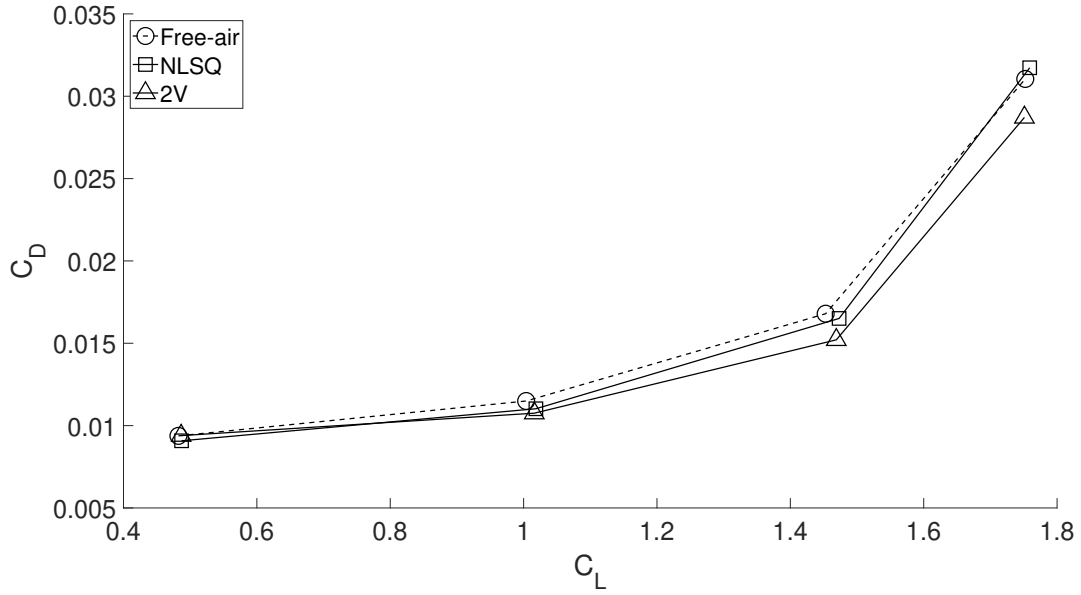

Figure 8 – Lift-Drag polars for the NACA 4415 at $H/D = 5$

While the 2V method was able to marginally better correct the lift, the differences were small. However, the NLSQ better captured the upwash interference due to its improved representation of the upwash velocity (see figure 9), and is significantly better at higher incidence. In two dimensions, the blockage and lift interference can be viewed as a scaling (blockage), and a rotation (upwash) of the velocity field. For high Lift/Drag bodies such as an aerofoil, small perturbations in the upwash interference can have significant effects on the drag due to the influence of the lift component. This illustrates that the increased accuracy afforded by the present method offers the potential for significant improvements over the 2V method for bodies such as those considered.

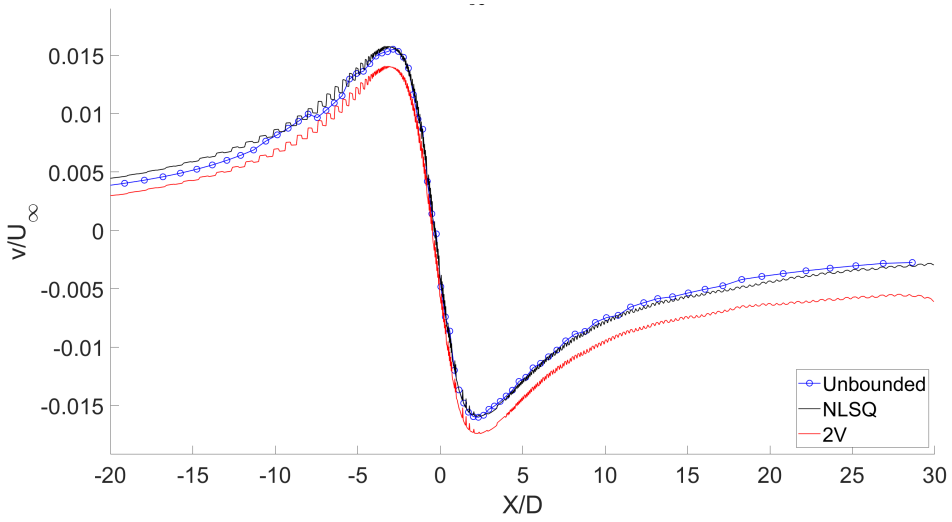

Figure 9 – Comparison of wall velocities around a 2D NACA 0012 aerofoil at $\alpha = 10°$, $Re = 10^6$ and $H/D = 10$, corrected using 2V and NLSQ methods.

4. Concluding remarks

The nonlinear least-squares optimised correction technique has demonstrated that it is capable of producing wall-effect corrections for 2D symmetric and lifting bodies including spoilers, with minimal computing requirements. Results demonstrate that the method is able to apply blockage corrections to bluff bodies in line with the existing two-variable method, and achieves superior drag corrections through an improved representation of upwash interference for lifting bodies. The additional singularities and degrees-of-freedom come at the expense of a requirement for a greater number of simultaneous experimental measurements (typically wall pressures) in order to obtain a unique solution. This, however, is no longer a limiting constraint as the cost of sensors has decreased significantly. Furthermore, the generality of the technique and the freedom to distribute potential flow singularities off the centreline may enable better simulation of highly-asymmetric geometries (such as model support struts) or asymmetric wall effects (as would be the case for yawed 3D models).
This work has been undertaken as part of a PhD investigating improvements to wind tunnel wall interference corrections. Future work will include the extension to three-dimensions and the application of the present correction method to experimental data for 2D and 3D bodies.

Acknowledgements

This work has been funded by QinetiQ Ltd. and The Boeing Company. The authors would like to thank Ian Smith, Head of Testing at QinetiQ 5m Wind Tunnel, and David Holler and Ashley Evans, Boeing, for their insights whilst developing this work.

5. Copyright Statement

References

[1] Barlow, J. B., Rae, W. H., and Pope, A., *Low-Speed Wind Tunnel Testing*, 3rd ed., Wiley, New York, 1999.

[2] Steinle, F., and Stanewsky, E., "Wind Tunnel Flow Quality and Data Accuracy Requirements," Tech. Rep. 184, AGARD, 1982.

[3] Ashill, P. R., and Keating, R. F. A., "Calculation of Tunnel Wall Interference from Wall-Pressure Measurements," *The Aeronautical Journal*, Vol. 92, No. 911, 1988, pp. 36–53. https://doi.org/10.1017/S0001924000021813.

[4] Hackett, J. E., Wilsden, D. J., and Lilley, D. E., "Estimation of Tunnel Blockage from Wall Pressure Signatures: A Review and Data Correlation," Tech. Rep. NASA CR-152241, NASA, 1979.

[5] Ewald, B. F. R. (ed.), *Wind Tunnel Wall Correction =: La Correction Des Effets de Paroi En Soufflerie*, No. 336 in AGARDograph, AGARD, Neuilly sur Seine, 1998.

[6] Iyer, V., Kuhl, D., and Walker, E., "Improvements to Wall Corrections at the NASA Langley 14 x 22-Ft Subsonic Tunnel," *21st AIAA Applied Aerodynamics Conference*, Vol. 2003–3950, Orlando FL, 2003, p. 15.

[7] Hackett, J. E., Cooper, K. R., and Perry, M. L., "Drag, Lift and Pitching Moment Increments Due to Wind Tunnel Wall Constraint: Extension to Three Dimensions," *ICAS 2000 Congress*, International Council of the Aeronautical Science, 2000, p. 16.

[8] Ulbrich, N., "The Real-Time Wall Interference Correction System of the NASA Ames 12-Foot Pressure Wind Tunnel," Tech. Rep. NASA/CR-1998 -208537, NASA, 1998.

[9] Iyer, V., and Everhart, J. L., "Application of Pressure-Based Wall Correction Methods to Two NASA Langley Wind Tunnels," *19 _ AIAA Applied Aerodynamics Conference*, AIAA, Annaheim, CA, 2001, p. 20. https://doi.org/10.2514/6.2001-2472.

[10] Ulbrich, N., "Direct Validation of the Wall Interference Correction System of the Ames 11-Foot Transonic Wind Tunnel," Tech. Rep. NASA/TM–2003-212268, NASA, May 2003.

[11] Garner, H. C., Rogers, E. W. E., Acum, W. E. A., and Maskell, E. C., "Subsonic Wind Tunnel Wall Corrections," 1966, p. 466.

[12] Anderson Jr., J., *Fundamentals of Aerodynamics Second Edition*, 2nd ed., McGraw-Hill, 1991.

[13] Ulbrich, N., and George, M., "Description of Panel Method Code Antares," Tech. Rep. NASA/CR-2000-209592, NASA, 2000.

[14] Coleman, T., and li, Y., "On the Convergence of Reflective Newton Methods for Large-Scale Nonlinear Minimization Subject to Bounds," *Math. Program.*, Vol. 67, 1994, pp. 189–224. https://doi.org/10.1007/BF01582221.

[15] Coleman, T. F., and Li, Y., "An Interior Trust Region Approach for Nonlinear Minimization Subject to Bounds," *SIAM J. Optim.*, Vol. 6, No. 2, 1996, pp. 418–445. https://doi.org/10.1137/0806023.

[16] Schlichting, H., and Truckenbrodt, E., *Aerodynamics of the Airplane*, McGraw-Hill, 1979.

[17] Catalano, P., Wang, M., Iacciarino, G., and Moin, P., "Numerical Simulation of the Flow around a Circular Cylinder at High Reynolds Numbers," *International Journal of Heat and Fluid Flow*, Vol. 24, 2003, pp. 463–469. https://doi.org/10.1016/S0142-727X(03)00061-4.

[18] Zdravkovich, M., *Flow around Circular Cylinders Volume 1: Fundamentals*, Vol. 1, Oxford University Press, 1997.

[19] Yeung, W. W. H., Xu, C., and Gu, W., "Reduction of Transient Adverse Effects of Spoilers," *Journal of Aircraft*, Vol. 34, No. 4, 1997, pp. 479–484. https://doi.org/10.2514/2.2216.

[20] Chow, R., and Dam, C. P. V., "Unsteady Computational Investigations of Deploying Load Control Microtabs," *Sept-Oct 2006*, 2006, pp. 1458–1469.

[21] Abbott, I., and Doenhoff, A. E. V., *Theory of Wing Sections*, dover ed., Dover Publiations Inc., 1959.

[22] Jespersen, D. C., Pulliam, T. H., and Childs, M. L., "OVERFLOW Turbulence Modeling Resource Validation Results," Tech. Rep. NAS-2016-01, NASA, NASA Ames Research Center, 2016.

[23] Gilbey, R., *Lift-Interference and Blockage Corrections for Two-Dimensional Subsonic Flow in Ventilated and Closed Wind-Tunnels*, Aerodynamics, Vol. 13, ESDU, 1995.

[24] Mokry, M., and Cooper, K., "Application of the Two-Variable Correction Method to Measurements in an Open-Jet Test Section," *45th AIAA Aerospace Sciences Meeting and Exhibit*, AIAA, Reno, Nevada, 2007. https://doi.org/10.2514/6.2007-962.